

**REDUCTION OF SOLID FUEL HYDROXYL-TERMINATED POLYBUTADIENE
COMBUSTION IN AIR USING A NON-PREMIXED COUNTERFLOW DIFFUSION
MODEL**

A Research Paper submitted to the Department of Aerospace Engineering
In Partial Fulfillment of the Requirements for the Degree
Bachelor of Science in Aerospace Engineering

By

Del Irving

May 1, 2022

On my honor as a University student, I have neither given nor received unauthorized aid on this assignment as defined by the Honor Guidelines for Thesis-Related Assignments.

ADVISOR

Harsha Chelliah, Department of Mechanical and Aerospace Engineering

ABSTRACT

Traditional hypersonic engines contain fuel and oxidizer in liquid form. By instead using external air as an oxidizer, weight is freed that can be used elsewhere such as for various systems or increased payload. Additionally, by utilizing solid fuel, specifically solid butadiene, instead of liquid fuel, the stability of the combustion reaction increases and reduces the change in center of gravity during flight. The goal of this project is to reduce the current model for a hybrid, air-breathing, hypersonic engine to a fraction of the time without sacrificing a significant amount of the precision in the code. Thus, a non-premixed counterflow diffusion model is constructed using the Cantera chemical database in Python. While for premixed models, laminar flame speed is the best optimization parameter for kinetic mechanisms, the ideal optimization parameter for non-premixed models is extinction strain rate. By integrating these models across all the small flamelets in the flame, a reduced model can be generated.

INTRODUCTION TO CANTERA

Cantera, an open-source chemical kinetics software program, was initially written by David Goodwin as a software toolkit of basic thermodynamic and chemical kinetic properties and as an overhaul of the Sandia National Laboratory's CHEMKIN (Smith, 2012, para. 8). The database was later developed by Raymond Speth, a researcher at the Massachusetts Institute of Technology who specializes in combustion and emissions, fuel production technology, and numerical methods (MIT Laboratory for Aviation and the Environment, 2022, para. 3). Cantera is used to solve for chemically reacting laminar flows, which is crucial when analyzing any injector or combustor system.

Originally written in the coding language C++, Cantera can be used from C++, Python, Matlab, or Fortran. For this independent project, the language Python was used to call the Cantera chemical database.

Cantera makes use of .cti files which are composed of all of the necessary information for a certain gas mixture, or mechanism, including all of the elements within the gas and the compounds, or species, that these elements can form. The file then further includes all of the species data necessary, which is made up of the atoms in each species, the thermodynamic data for that species, and the transport data for that species. Thermodynamic data commonly comes in two sets, one at a low temperature range and the other at a high temperature range. This data is modeled by a seventh order polynomial fit pulled from NASA parameterizations (Cantera Developers, 2022, para. 11). Figure 1 pictures species data for the species H₂O, directly pulled from the mechanism file grimech30.cti which is an optimized mechanism for modeling natural gas combustion. Within the ‘thermo’ data, two specific sets of two values and then seven values can be seen. The first two are the temperature range in degrees Kelvin, so 200K to 1000K for the first range, and the last seven values are the coefficients for the seventh order polynomial, or septic equation ($Ax^6+Bx^5+Cx^4+\dots$), that models the thermodynamic properties of the species.

```

species(name='H2O',
        atoms='H:2 O:1',
        thermo=(NASA([200.00, 1000.00],
                      [ 4.19864056E+00, -2.03643410E-03, 6.52040211E-06,
                        -5.48797062E-09, 1.77197817E-12, -3.02937267E+04,
                        -8.49032208E-01]),
                NASA([1000.00, 3500.00],
                      [ 3.03399249E+00, 2.17691804E-03, -1.64072518E-07,
                        -9.70419870E-11, 1.68200992E-14, -3.00042971E+04,
                        4.96677010E+00])),
        transport=gas_transport(geom='nonlinear',
                                 diam=2.605,
                                 well_depth=572.4,
                                 dipole=1.844,
                                 rot_relax=4.0),
        note='L8/89')

```

Figure 1: Thermodynamic and Transport Data in .cti file. Screenshot from the file grimech30.cti of specifically the thermodynamic and transport data for the H₂O species, including two seventh order NASA parametrizations and geometric data about the molecule.

Below the thermodynamic data is the transport data which includes data about the physical properties of the species such as the Lennard-Jones collision diameter ('diam') in Angstroms, the Lennard-Jones well depth ('well_depth') in Kelvin, the permanent dipole moment ('dipole') in Debye, and the rotational relaxation collision number at a temperature of 298K ('rot_relax') which is dimensionless (Cantera Developers, 2021, para. 22). This data is listed for every species within the mechanism, followed by the reaction data which can be seen in Figure 2 from the same grimech30.cti file for the reaction of oxygen and diatomic hydrogen.

```

# Reaction 3
reaction('O + H2 <=> H + OH', [3.870000e+04, 2.7, 6260.0])

```

Figure 2: Reaction Data in .cti file. Screenshot from the file grimech30.cti of specifically the reaction data for the reaction of monatomic oxygen and diatomic hydrogen, including the three coefficients necessary to determine the rate constant through the Arrhenius equation.

The string at the beginning of the reaction statement represents the reaction taking place while the array of three numbers represents coefficients A, b, and E in the Arrhenius equation which is written as:

$$k = AT^b e^{(-E/RT)}$$

where T is the temperature, R is the universal gas constant, and k is the rate constant that is being solved for (Cantera Developers, 2021, para. 23).

It is important to note that Cantera is switching over from .cti files to .yaml files in the near future, but for the purpose of this project only .cti files were used for the applied mechanisms.

BASICS OF COMBUSTION ANALYSIS

Before analyzing the more complex counterflow diffusion flames which are the end goal of this project, the basics of combustion analysis must first be understood. First, freely propagating, adiabatic, one dimensional flames are used to understand the basics of combustion. Adiabatic implies that there is no heat exchange between the system and its environment, so adiabatic flame temperature is an excellent measure of the temperature of the products of combustion after all of the chemical reaction heat released has heated those products. The first code, the output of which can be seen in Figure 3, models this adiabatic flame temperature as a function of equivalence ratio. Equivalence ratio is a ratio of the actual fuel-to-air ratio to the stoichiometric fuel-to-air ratio. Stoichiometric combustion occurs when all of the oxygen in the reaction is consumed, meaning there is no diatomic oxygen, O_2 , in the products. At an equivalence ratio equal to 1, the combustion is stoichiometric. An equivalence ratio less than one denotes a lean combustion with excess air compared to an equivalence ratio of more than one which denotes a rich combustion with excess fuel, known as a fuel rich or incomplete combustion (Colorado State, 2022, para. 5).

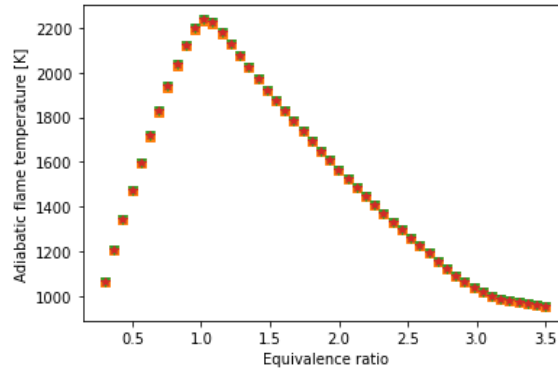


Figure 3: Adiabatic Flame Temperature. Adiabatic flame temperature for four various mechanisms as a function of equivalence ratio.

Figure 3 models the adiabatic flame temperature in Kelvin as a function of equivalence ratio for four different mechanisms: grimech30.cti, AramcoMech2_C4.cti, AramcoMech20_noTransport.cti, and gri30.yaml. For all four mechanisms, the plot is exactly the same, validating each mechanism. It can be shown from Figure 3 that adiabatic flame temperature for a lean combustion increases roughly linearly until a nearly stoichiometric combustion is achieved, at which point the combustion becomes fuel rich and adiabatic flame temperature begins to decrease exponentially. For this combustion, a gas mixture of 1 part O_2 and 3.76 parts N_2 , or a standard air mixture, was used. From Figure 3 it appears that the peak adiabatic flame temperature actually occurs slightly past the stoichiometric combustion point, meaning the highest temperature is a product of a fuel rich combustion. This is most likely related to products of the combustion diffusing back to the reactant side of the flame to be combusted again by the excess fuel. More often than not, lean combustion is used in reality in order to ensure complete combustion.

The next feature of combustion reactions that must be understood is ignition delay. From the time when the gas is released to the time combustion occurs, there is a slight gap in time barely a ten-thousandth of a second as depicted in Figure 4.

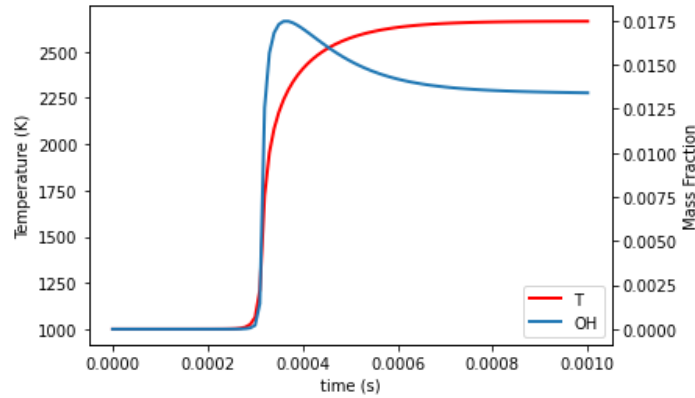


Figure 4: Temperature and Mass Fraction. Temperature and mass fraction of OH as a function of time, representing the ignition delay that takes place in the cold region before the flame structure and combustion.

Figure 4 also models the mass fraction of OH, which helps to determine the ignition delay. There are many ways to calculate the point when ignition occurs, but for the purpose of this project the ignition point is defined as the first point where the temperature increases 50K above the initial temperature, or right around 0.0003 seconds for this example. Although miniscule, it can be shown that ignition delay varies as a function of temperature and pressure. As both the temperature and pressure increase, ignition delay time decreases exponentially, and can be linearized by plotting the log of the ignition delay as a function of the inverse of the temperature or pressure.

Knowledge of combustion data such as equivalence ratio and ignition delay time are extremely useful in not only developing more complex models, but also in understanding what is occurring in chemically reacting laminar flows.

FLAME SPEED

From ignition delay the combustion analysis goes on to calculate flame speed, a very important metric in the scope of this project. Flame speed is the measured rate of expansion of the flame front or flame structure in a combustion reaction, and varies greatly depending on the

fuel species being analyzed. Figure 5 pictures the flame speed in meters per second as a function of equivalence ratio for two different fuel species, CH_4 on the left and H_2 on the right.

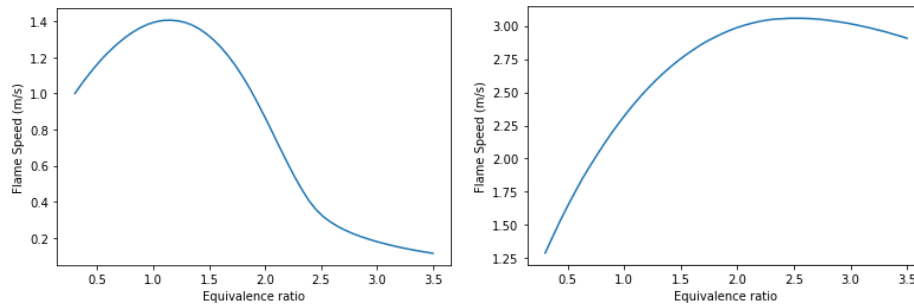


Figure 5: Flame Speed. Flame speed for two different fuel species as a function of equivalence ratio, with CH_4 as the fuel species on the left and H_2 as the fuel species on the right.

Methane (CH_4) is a simple hydrocarbon and models the basics of the more complex hydrocarbon fuels that will eventually be studied, but its flame speed function differs greatly from that of a pure hydrogen fuel. The flame speed for a methane burning combustion peaks at a roughly stoichiometric reaction while the flame speed of hydrogen peaks at a very fuel rich combustion at an equivalence ratio of almost 2.5. Flame speed also presents an opportunity to discuss the difference between the two prevalent models in the combustion community: the mixture averaged model and the multi component model. Figure 6 looks at the same hydrogen fuel species, but for both a mixture averaged and multi component model.

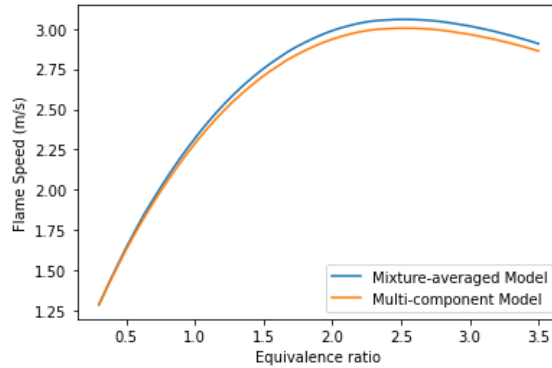


Figure 6: Flame Speed for Two Various Modeling Methods. Flame speed as a function of equivalence ratio for a more precise multi-component model and for the favored mixture-averaged model that will be used throughout the project.

Although the multi component model is more complex and precise than the mixture averaged model, it is clear from Figure 6 that the two do not differ significantly, especially at equivalence ratios around 1 which will be analyzed during the course of the project.

Additionally, due to the simplicity of the mixture averaged model, computation times are much shorter and conducive to the goal of the project which is to reduce the run time of the current program and will thus be used instead of multi component modeling for the duration of the code.

Getting back into flame speed, this data aids in setting up the initial speed of the gas as well in order to hold the flame structure steady. A moving flame structure is much more difficult to analyze than a stagnant flame, so the goal of calculating flame speed is to counter this motion by setting the incoming gas speed accordingly. As the flame expands towards the gas during combustion, a gas at the right speed will hold the flame steady, making it possible to analyze mass fractions of all species within the reaction on both sides of the flame.

MASS FRACTIONS AND HEAT RELEASE

Once the flame is stabilized, it is possible to analyze the mass fractions of the reactants and the products on either side of the flame structure. Mass fraction is a dimensionless value which represents the mass of a particular species compared to the mass of all the other species

involved in combustion. These values can be seen in Figure 7 which analyzes the combustion of methane and air.

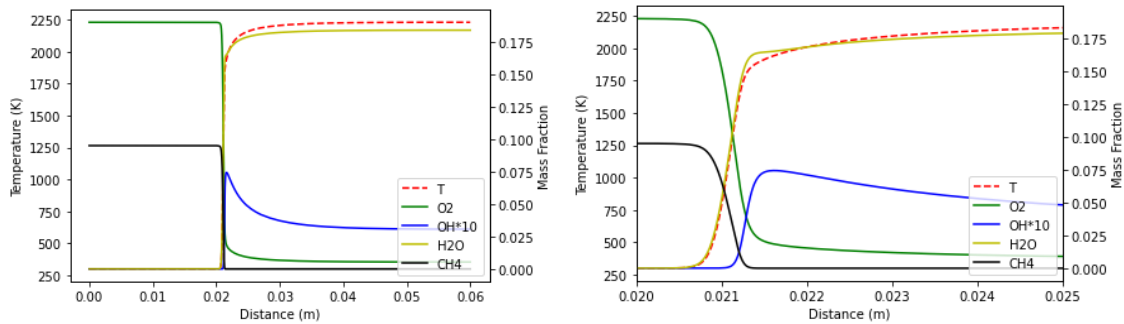


Figure 7: Mass Fraction. Mass fractions and temperature as a function of distance across the combustion chamber with the left image showing the full combustion chamber and the right showing a closer view towards the flame structure.

The first image on the left depicts the entire distance across which the combustion is analyzed, from 0 to 6 centimeters. It is clear in this image where the flame structure sits, right around 2.1 centimeters from the left side, as is evident from the drastic decrease in the mass fractions of the reactants, the increase in the mass fractions of the products, and the sharp increase in temperature which is denoted by the dashed red line. However, it is difficult to note the effects of diffusion of species across the flame structure from this full view which is where the image on the right becomes very helpful.

The second image on the right focuses on the millimeters around the flame structure and allows for a much better analysis of the diffusion taking place through the flame front. In pure combustion, the mass fractions of the reactants would simply decrease immediately to zero after crossing the flame, however here for example the mass fraction of oxygen begins to decrease slightly before the flame and then continues to decline past the flame structure on the other side. This is due to the fact that some oxygen molecules diffuse through the flame structure without

undergoing combustion and make it so the mass fraction is slightly above equilibrium and slowly decreases to the true value further from the flame.

In addition to the mass fractions of the species being analyzed in the combustion, the heat release of the combustion itself can also be modeled. Figure 8 similarly models a combustion of methane and air first for the entire system and then on the right for a more select window that looks specifically at the millimeters around the flame structure.

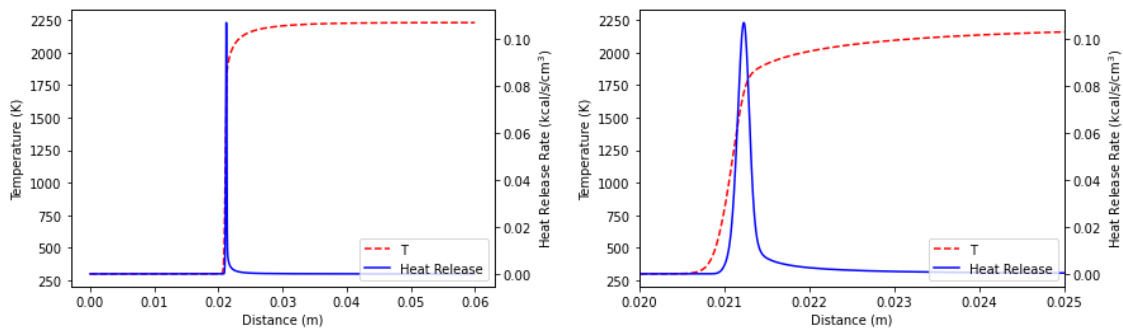


Figure 8: Heat Release. Heat release and temperature as a function of distance across the combustion chamber with the full combustion chamber shown on the left and a section closer to the flame structure shown on the right.

From the image on the left it is clear that the majority of the heat released occurs right at the flame structure where the temperature increases from the initial value to the final value. When the analyzed section is zoomed in to the area right around the flame it is clear that there is still a bit of heat release that occurs right after the flame where the temperature is still slightly increasing to equilibrium, but the majority of the heat release is due to the combustion right at the flame line.

TYPES OF FLAME MODELS

Up until this point all of the analysis done has been on one dimensional open flames. This is simply where the fuel and oxidizer, or reactants, are pushed through a flame structure where combustion occurs, as is shown in Figure 9.

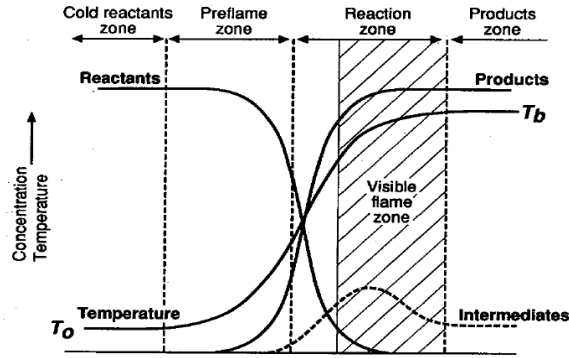


Figure 9: One-dimensional Open Flame. Depiction of a standard one-dimensional open flame modeling the various sections throughout the combustion chamber as well as the relative concentrations of the reactants, products, and intermediates with the temperature curve plotted on top. (Rathod, 2020, para. 2)

From Figure 9, it can be shown that a one dimensional open flame has four main regions: the cold reactants zone where the fuel and oxidizer flow before the temperature has increased, the preflame zone where the temperature begins to increase and mass fractions begin to vary slightly before the flame, the reaction zone where the visible flame structure exists and the majority of combustion takes place, and the products zone where the mass fractions of the products of combustion of the fuel and the oxidizer as well as the temperature begin to reach equilibrium or a constant value. Figure 9 and Figure 7 are very similar, and from this it can be seen that intermediates like in the reaction in Figure 7 are still important to the overall combustion and demonstrate why the 39 species butadiene model will later be necessary.

From here on, all of the models being used will instead utilize a counterflow diffusion model, an example of which can be seen in Figure 10.

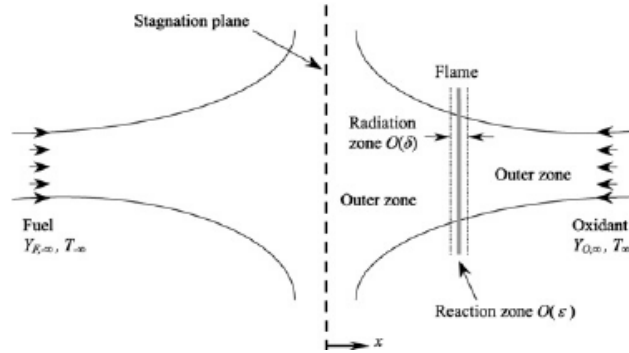


Figure 10: Non-premixed Counterflow Diffusion Flame. Depiction of a standard non-premixed counterflow diffusion model with the fuel flowing in from the left and the oxidant flowing from the right, creating a stagnation plane in the middle while the flame sits closer to the oxidizer. (Wang, 2007, para. 1)

In a counterflow diffusion model, specifically the non-premixed counterflow diffusion model in Figure 10, the fuel and oxidizer approach each other from opposite directions, creating a stagnation plane in the middle where the two meet. The flame structure for a non-premixed counterflow diffusion model usually occurs closer to the oxidizer side, and is parallel to the stagnation plane. In twin premixed counterflow flames, the geometry is the same but instead of having the fuel and the oxidizer separated, each inlet contains both the fuel and the oxidizer initially. For the purpose of this project, non-premixed counterflow diffusion flames such as the one in Figure 10 will be utilized.

From such flames, two pieces of data will be extremely useful. First the axial velocity of the flame, or the velocity perpendicular to the stagnation plane, can be measured at each point between the fuel inlet and the oxidizer inlet. Second, the temperature at each point between the two inlets will be very important information. These two values will be modeled against distance and will vary with changes in inlet velocities.

PEAK TEMPERATURE VS. STRAIN RATE

Figure 11 is included to put a visual to the axial velocity and temperature of the counterflow diffusion model as a function of distance with an initial fuel inlet velocity of 5 meters per second.

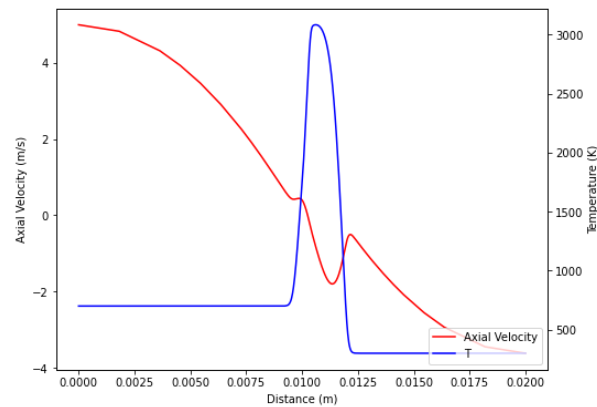


Figure 11: Axial Velocity and Temperature. Axial velocity and temperature for a non-premixed counterflow diffusion flame as a function of distance across the combustion chamber.

As the fuel travels to the stagnation point in the middle, the axial velocity gradually slows down towards zero meters per second at the stagnation plane. Right as the fuel reaches the beginning of the flame structure, denoted by the spike in temperature, the axial velocity increases as it crosses through the flame, then within the flame itself continues to decrease, and then increases sharply again when exiting the flame only to continue decreasing until approaching the oxidizer inlet. Although the axial velocity of the flame is decreasing, it should be noted that after crossing the stagnation plane, the magnitude of the axial velocity, or speed of the particles, actually increases since now the flow is going in the opposite direction due to the oxidizer inlet firing against the fuel inlet.

Looking at the temperature profile for the counterflow diffusion model, the initial temperature of the fuel remains constant until reaching the flame structure, at which point the temperature drastically increases to a peak temperature near the center of the flame structure, and

then decreases to the initial oxidizer temperature after crossing the flame. For most models, the initial fuel temperature is higher than or equal to the initial oxidizer temperature.

From Figure 11 the most important pieces of information to analyze are the peak temperature, which occurs within the flame structure, and the strain rate. The strain rate is the greatest rate of change in axial velocity that occurs, or “the oxidant-side velocity gradient upstream of the flame” (Fisher et al., 1997, p. 1). By varying the initial velocity of the fuel inlet, values can be generated for the peak temperature which is then modeled as a function of the strain rate in Figure 12.

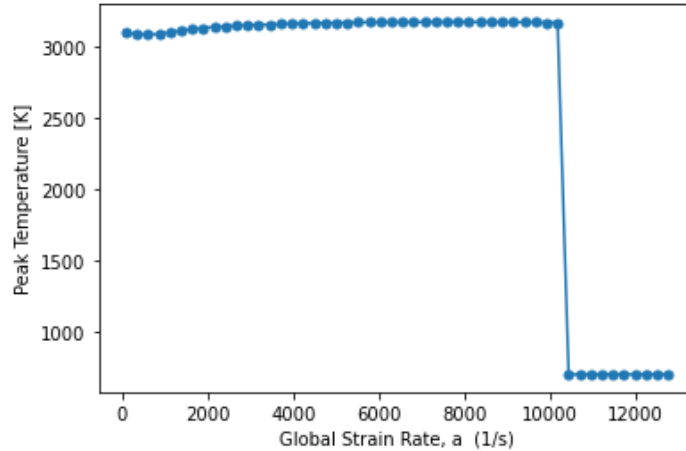


Figure 12: Peak Temperature vs. Strain Rate. Maximum temperature for a non-premixed counterflow diffusion flame as a function of global strain rate.

As global strain rate, which has an inverse time scale, increases, peak temperature remains roughly constant often with a slight decline in peak temperature at higher strain rates. The most evident piece of information that can be gathered from relations like Figure 12 is that there is a certain strain rate above which the peak temperature drops down to the initial fuel temperature, meaning the flame never ignites and combustion cannot occur. This is referred to as the extinction strain rate. “Extinction occurs when [initial] fuel and oxidant flow rates are increased above certain values. An intuitive interpretation of this phenomenon is that the flame is

blown out when chemical reactions can not occur fast enough to maintain a sufficient pool of reactive species against the flow of incoming reactants" (Fisher et al., 1997, p. 1).

Extinction strain rate is a very useful metric to characterize fuel and oxidizer combustion, but can be difficult to calculate since it can only be analyzed forwards, meaning it has to be calculated from the last point from before the flame was extinguished. This means the piece of the function in Figure 12 on the right from after the flame has been extinguished cannot be used when calculating this value.

DIFFUSION FLAME EXTINCTION

Before the final butadiene-air model is analyzed, a more simple ethylene-air model is first utilized to confirm that the code is successfully working. As is stated in Fisher et al. (1997), the strain rate is analyzed in the cold region on the oxidizer inlet sides and modeled against temperature to create Figure 13 (p.1).

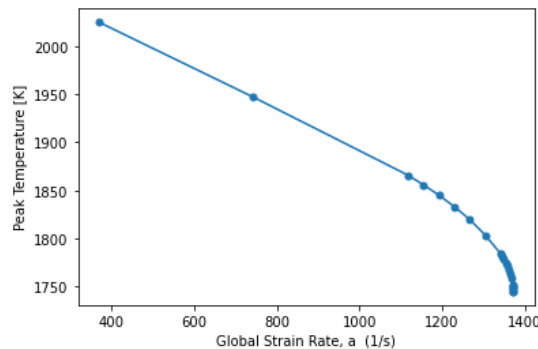


Figure 13: Peak Temperature for Ethylene. Peak temperature as a function of global strain rate for the fuel species ethylene in a non-premixed counterflow diffusion model.

This model of peak temperature as a function of global strain rate can be compared to the model created in the paper by Sarnacki et al. (referred to as Sarnacki from this point on) which analyzes various inlet diameters which is beyond the scope of this project. The Sarnacki model can be seen in Figure 14.

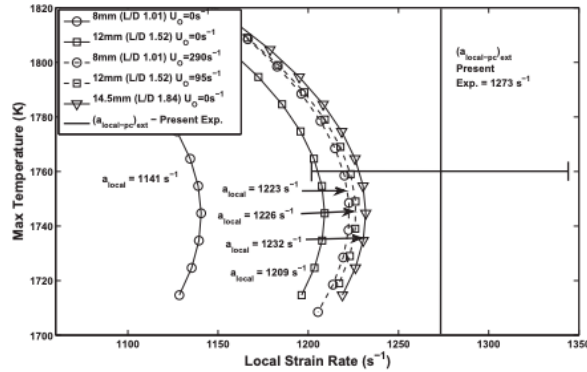


Figure 14: Max Temperature vs. Local Strain Rate for Butadiene. Max temperature modeled as a function of local strain rate for a number of various inlet nozzle diameters. (Sarnacki, 2012, p.1035)

The slight differences between the two models can be mainly attributed to the fact that the Sarnacki model utilizes butadiene as the fuel where the model created still uses ethylene as the fuel. Beyond this the model created for this project stops calculating after the peak strain rate where the Sarnacki paper continues with further data points beyond the maximum local strain rate, making the extinction strain rate calculation more accurate. Outside of these clear differences, the model created for the project is not far off from the Sarnacki model and confirms that the code is developed enough to switch the fuel species from ethylene to the final goal of the 39 species butadiene mechanism in Figure 15.

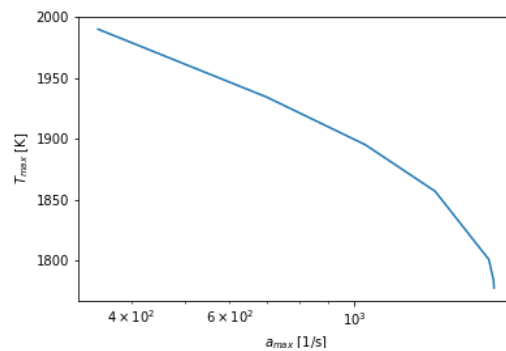


Figure 15: Max Temperature vs. Strain Rate for Butadiene. Max temperature as a function of global strain rate for the fuel species butadiene.

By switching the fuel from ethylene to butadiene, the values now match much more closely to the Sarnacki results.

MIXTURE FRACTION AND COMPARISON TO CIOTTOLI

Now that the butadiene fuel has been implemented, the next step is to compare the results of the code to the models produced in the paper by Ciottoli et al. (referred to as Ciottoli from here on). In the Ciottoli models however, the temperature and mass fraction functions previously analyzed no longer have distance in meters on the x-axis, but instead are modeled as a function of mixture fraction. Mixture fraction is a much more normalized metric which allows for ease of comparison since the flame front may have varying widths with different input parameters. By using mixture fraction on the x-axis the flame size is normalized and it becomes much easier to compare multiple results.

Mixture fraction is calculated as a function of the weight of each element, the weight of each species, and the mass fraction of that species. For example, the carbon portion of the mixture fraction is written as:

$$Z_C = \frac{W_C}{W_{C4H6}} \cdot 4 \cdot Y_{C4H6} + \frac{W_C}{W_{CO2}} \cdot 1 \cdot Y_{CO2} + \frac{W_C}{W_{CO}} \cdot 1 \cdot Y_{CO} + \dots$$

Here W_C is the weight of carbon, W_{C4H6} is the weight of butadiene, the coefficient is the number of carbon atoms in the species, and Y_{C4H6} is the mass fraction of butadiene. More species may be added to make the model more accurate. These values for carbon, oxygen, and hydrogen are then combined using:

$$Z_x = Z_C + Z_H - 2Z_O$$

And produce a final mixture fraction at each point, i, using:

$$Z = \frac{Z_x[i] - Z_x[end-1]}{Z_x[0] - Z_x[end-1]}$$

This produces a dimensionless, normalized value which approaches 0 at the oxidizer stream and 1 at the fuel stream.

With the mixture fraction calculated, functions of temperature and mass fractions can then be generated. Plots are generated at a constant pressure of 36 bars and can be seen in Figures 16 and 17.

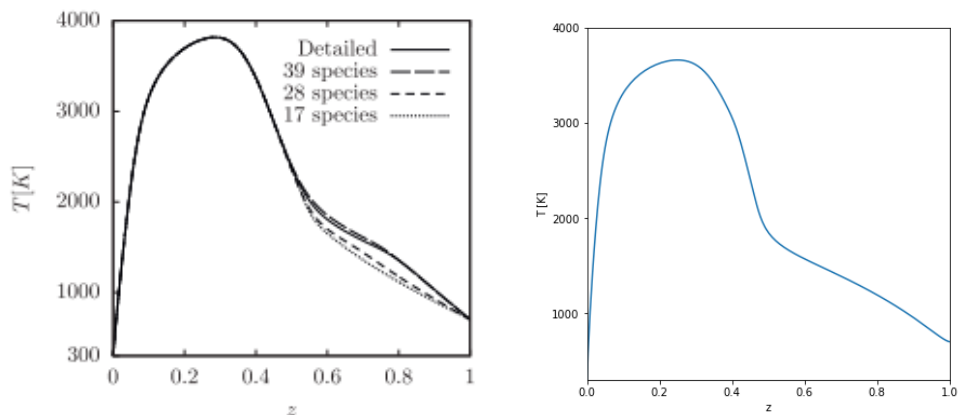


Figure 16: Temperature vs. Mixture Fraction. Temperature as a function of mixture fraction from the Ciottoli model on the left which includes a function for variously detailed mechanisms and the project generated model on the right for the 39 species mechanism, both using the fuel species butadiene at a constant pressure of 36 bars. (Ciottoli, 2017, p. 88)

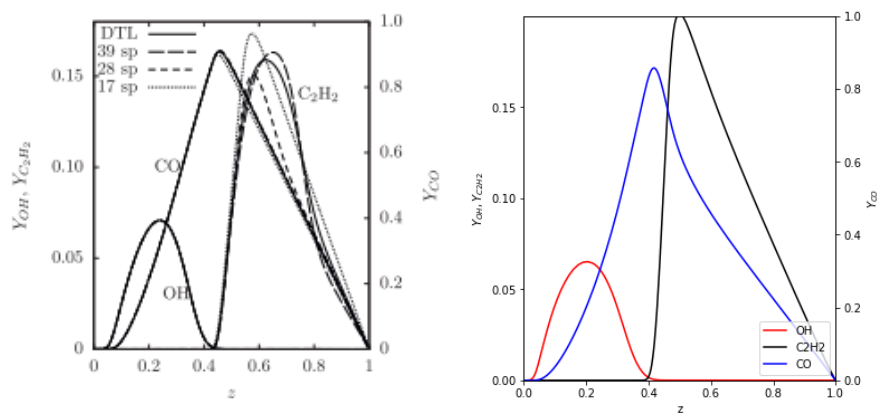


Figure 17: Mass Fraction vs. Mixture Fraction. Mass fraction as a function of mixture fraction for three species (OH, C₂H₂, CO) from the Ciottoli model on the left which includes a function for variously detailed mechanisms and the project generated model on the right for the 39 species mechanism, both using the fuel species butadiene at a constant pressure of 36 bars. (Ciottoli, 2017, p. 88)

Figure 16 shows the Ciottoli model on the left for the temperature as a function of mixture fraction for a 17 species mechanism of butadiene, a 28 species mechanism, the target 39 species that this project is analyzing, and a more detailed mechanism which includes all of the species involved in the combustion. To the right in Figure 16 is the same function generated with the project code for the 39 species mechanism of butadiene. These models are extremely similar and help to verify that the code exceeds at plotting the temperature as a function of mixture fraction.

Figure 17 also has the Ciottoli model on the left for the mass fractions of a few select species as a function of the mixture fraction for the same 17 species, 28 species, 39 species, and detailed mechanisms. The species analyzed are OH, C₂H₂, and CO. The right model in Figure 17 shows the project code generated plot of the same function, which models the OH mass fractions very well and hits upon the trends for the mass fractions of C₂H₂ and CO. The reason that this model does not replicate the Ciottoli models is because the mixture fraction, unlike the butadiene mechanism, only includes the ten most abundant species. This leaves out the mass fractions of several smaller species that in total add up to distort the mass fractions of C₂H₂ and CO from the correct values generated in the Ciottoli model.

In order to make the models more accurate, the mixture fraction must be calculated using all 39 species that are included in the butadiene mechanism of choice for this project. Once this small step is completed, the model will be set to run just as the more precise Naval Research Laboratory code already achieves but at a much faster computational rate.

FURTHER APPLICATIONS

Once this change is made to reflect all of the species that should be analyzed in the combustion of solid butadiene and air in the hybrid, air-breathing engine, the code can be used to

generate results for further applications. For example, a different mechanism studying a more complex hydrocarbon than butadiene may be studied using this code to see if the extinction strain rate varies favorably or if there is a better oxidizer than pure air for the efficiency of this system. Regardless, this project achieved the goal of reducing the computational time for the combustion analysis of solid butadiene in a hybrid, air-breathing, hypersonic engine through the use of the Cantera software package for Python.

REFERENCES

- Cantera Developers. (2022). *Elements and species*. <https://cantera.org/tutorials/cti/cti-species.html>
- Cantera Developers. (2021). *CTI class reference*. https://cantera.org/documentation/docs-2.5/sphinx/html/cti/classes.html#cantera.ctml_writer.gas_transport
- Ciottoli, P. P., Galassi, R. M., Lapenna, P. E., Leccese, G., Bianchi, D., Nasuti, F., Creta, F., & Valorani, M. (2017). CSP-based chemical kinetics mechanisms simplification strategy for non-premixed combustion: An application to hybrid rocket propulsion. *Combustion and Flame*, 186, 83-93. <https://www.sciencedirect.com/science/article/abs/pii/S0010218017302912>
- Colorado State. (2022). *Stoichiometry*. [https://www.engr.colostate.edu/~allan/thermo/page9/page9.html#:~:text=The%20equivalence%20ratio%20is%20defined,\(O2\)%20in%20the%20products](https://www.engr.colostate.edu/~allan/thermo/page9/page9.html#:~:text=The%20equivalence%20ratio%20is%20defined,(O2)%20in%20the%20products)
- Fisher, E. M., Williams, B. A., & Fleming, J. W. (1997). Determination of the strain in counterflow diffusion flames from flow conditions. *Proceedings of the Eastern States Section of the Combustion Institute*, 191-194. https://www.nist.gov/system/files/documents/el/fire_research/Fisher-Determination-of-the-strain-in-counterflow-diffusion-flames-from-flow-conditions.pdf
- MIT Laboratory for Aviation and the Environment. (2022). *Raymond Speth*. <https://lae.mit.edu/team/raymond-speth/>
- Rathod, R. (2020). 1D flame speed analysis. *Skill Lync*. <https://skill-lync.com/student-projects/1d-flame-speed-analysis-emsp-cantera-skill-lync-medium>
- Sarnacki, B. G., Esposito, G., Krauss, R. H., & Chelliah, H. K. (2012). Extinction limits and associated uncertainties of nonpremixed counterflow flames of methane, ethylene, propylene and n-butane in air. *Combustion and Flame*, 159(3), 1026-1043. https://www.sciencedirect.com/science/article/pii/S0010218011002823?casa_token=LUHWXtF_UPkAAAAA:5M_0yZunPPdAkHjDJaF62C4biW2U-wz9ZcH6gDQWGgtjqtL0V_Wfsh81CDgPMbTPNg52YdjaIg
- Smith, D. (2012, November 12). Caltech mourns the passing of David G. Goodwin. *Caltech*. <https://www.caltech.edu/about/news/caltech-mourns-passing-david-g-goodwin-37485>

Wang, H. (2007). Extinction of counterflow diffusion flames with radiative heat loss and nonunity Lewis numbers. *ResearchGate*. https://www.researchgate.net/figure/Schematic-of-a-counterflow-diffusion-flame_fig1_255143554